IEEE Access
Multidisciplinary | Rapid Review | Open Access Journal

Received July 26, 2020, accepted August 7, 2020, date of publication August 11, 2020, date of current version August 27, 2020.

Digital Object Identifier 10.1109/ACCESS.2020.3015763

Analytical Analysis and Design of an Advanced Differential-Mode Current Sensor for Insulation Monitoring for Industrial Electrical Assets

GEYE LU, (Student Member, IEEE), YANG WU, (Graduate Student Member, IEEE), AND PINJIA ZHANG, (Senior Member, IEEE)
Department of Electrical Engineering, Tsinghua University, Beijing 100084, China

Corresponding author: Pinjia Zhang (pinjia.zhang@ieee.org)

This work was supported by the National Natural Science Foundation of China under Grant 51777112, Grant 51822705, and Grant 61703227.

ABSTRACT Some industrial incidents are attributed to insulation degradation of electrical assets. The leakage current can be a crucial indicator for online insulation monitoring of asset. To realize per-phase monitoring, the measurement accuracy of milliampere-level leakage current is limited by the strong load current noises. This article proposes an advanced current sensor with a dual-core topology based on differential-mode (DM) measurement. An analytical model of magnetic field of the dual-core sensor is originally presented. It helps clarify the significances of the inner core in filtering noises and reducing the influence of system operation and cable positioning. Then, a comprehensive design procedure is fully investigated by selecting the optimal position and approach for magnetic field detection, and a high-speed and low-noise signal conditioning circuit is presented. The proposed current sensor is tested in the laboratory. Experimental results indicate that measurement errors can remain within 0.1mA in the testing scope, where the load current is up to 100A and the DM current varies from 0-7mA. The proposed sensor is further validated with superior performance compared with two commercial industrial sensors. The contribution of this article lies in providing the analytical analysis and design of a novel DM current sensor for leakage current measurement, which achieves online per-phase insulation monitoring for industrial electrical assets.

INDEX TERMS Electrical assets, monitoring, current sensor, differential mode (DM), leakage current, analytical model, magnetic field detection.

I. INTRODUCTION

Industrial power system faces the risk of low-automatized and low-secure operation. New technical difficulties are brought in the system reliability with the large-scale integration of renewable energy resources and varied industrial loads [1]. Industrial electrical assets, such as transformers and electrical machines, are reported with incidents that often evolve from insulation deterioration [2]–[5]. The fault isolation and recovery time could be too long to achieve system reconstruction and self-healing, by relying on maintenance regulations and relay protections. Thus, online insulation monitoring for industrial electrical assets has been the principal focus on reducing outage risk and improving supply quality.

The transformers serve as core assets connecting the grid and the load while electrical machines play a significant role in variable-speed load applications. Their insulation systems deteriorate due to the prolonged operating period. Among the existing popular techniques for industrial electrical assets, the leakage current can be used as an effective indicator for online insulation monitoring [6]. Fig. 1 illustrates the equivalent circuit of the ground-wall (GW) insulation system of the electrical machine. Under the excitation of operating voltage, the leakage current flows through the GW insulation into the ground, which gradually increases with insulation ageing. For a healthy medium motor, the leakage current at power frequency is conventionally up to dozens of milliamperes [7].

The associate editor coordinating the review of this manuscript and approving it for publication was Yilun Shang.

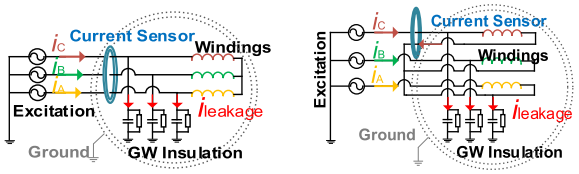

(a) CM measurement (b) DM measurement

FIGURE 1. Two measurement approaches for leakage current of the electrical machine.

The leakage current of a healthy industrial transformer is conventionally in a few milliamperes [8].

Reliable and accurate sensing technique for such a milliampere-level leakage current measurement is crucial to online insulation monitoring for electrical assets. There are two main approaches, based on common-mode (CM) measurement and differential-mode (DM) measurement, respectively. In Fig. 1(a), the current sensor encircles the cables of three phases, so that CM measurement is informative for the overall insulation condition of the machine [9]–[13]. By contrast, DM measurement is capable of assessing per-phase insulation condition [14]–[17], since the inlet and outlet cables of the winding go through the current sensor together, as shown in Fig. 1(b). Under such two modes, the current density inside the sensor is determined by the leakage current, since these produced by the load currents in two cables are equal and opposite. Hence, online insulation monitoring can be realized based on leakage current measurement in the presence of large load current noises.

At present, there are many products for small current measurement on a single wire, which are well qualified in measuring the leakage current of the insulators and the transformer core [18]–[20]. However, they may fail in ***online*** insulation monitoring in this application of Fig. 1, due to a lack of focus on several crucial effects. *For one thing*, the currents in cables include large load current, besides the milliampere-level leakage current. The magnetic field caused by the load current heavily masks that by the leakage current. The accuracy and sensitivity of leakage current measurement are limited by such intensive noises. *For another*, under both CM and DM measurement, the magnetic field is spatially distributed and significantly dependent on cable positioning and system operation. The root cause for unsatisfactory measurement by regular sensors in this application is the incapacity of eliminating the effects of uncertain operating factors.

To realize online per-phase insulation monitoring for industrial electrical assets based on leakage current measurement, a novel current sensor with a dual-core topology is proposed [17]. The inner core plays a significant role in filtering load current noises and the outer core realizes leakage current measurement in a sensitive manner. As a continuation of the previous work, this article contributes to solving the following three issues of DM leakage current measurement. *Firstly*, analytical analysis of magnetic field distribution has not been presented so far for the current sensor with dual-core topology. The analytical model should be provided to quantify the filtering effect of the inner core under strong load current noises. *Secondly*, the sensor performance is subject to several factors in the field, including changeable system operation, asymmetrical cable positioning and the axial dimension of the cores. These effects need to fully investigated in support of the sensor design. *Thirdly*, a comprehensive design procedure is expected by taking into consideration the optimal position and approach for magnetic field detection. In particular, an elaborate signal conditioning circuit should be presented to achieve a high-speed and low-noise signal output related to the measured DM leakage current.

This article is structured as follows. In Section II, the analytical model of magnetic field distribution of the sensor with two concentric cores is derived and validated using finite element analysis (FEA). In Section III, several influencing factors are discussed on the sensor performance. Section IV displays the design procedure by investigating the optimal detection approach and presenting the signal conditional circuit. Section V shows the experimental results of the sensor prototype and compares with two commercial industrial products. Section VI concludes this article. The main contribution of this article lies in proposing an advanced DM current sensor that is capable of per-phase online insulation monitoring for industrial electrical assets. The leakage current can be measured in a more accurate and sensitive manner under strong load current noises. Besides, the analytical analysis provides the guide of geometric configuration and benefits the procedure of designed sensor.

II. ANALYTICAL MODEL OF DUAL-CORE SENSOR

A. TOPOLOGY OF THE DUAL-CORE SENSOR

The dual-core sensor involves a filtering core and a detection core that are concentric, whose geometric illustration is given in Fig. 2. In this section, assume that a pair of cables are placed symmetrically with respect to the center point of the cores. Appropriate insulation distance is considered between the inlet and outlet cables of the monitored asset, according to the insulation requirement.

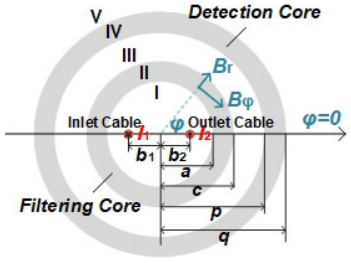

FIGURE 2. Geometric illustration of the dual-core current sensor.

Referring to Fig. 1(b), the conducting current in the inlet cable contains two components, namely the load current and the leakage current. The conducting current in the outlet cable is equal to the load current. The leakage current can be referred to as the DM current. The analytical model is built to compute the magnetic field produced by all conducting

TABLE 1. Medium property and geometric configuration.

Unit	Quantity	Symbol	Specification
Filtering Core	Inner diameter	$2a$	72 mm
	Outer diameter	$2c$	90 mm
Detection Core	Inner diameter	$2p$	117 mm
	Outer diameter	$2q$	135 mm
Cable Positioning	Inlet cable	b_1	25 mm
	Outlet cable	b_2	25 mm
Permeability	Air	u_0	$4\pi\times10^{-7}$ H/m
	Core	u_r	$4\pi\times10^{-3}$ H/m

currents in cables. The information of medium properties, geometric configuration and cable positioning used hereinafter is listed in Table. 1.

B. ANALYTICAL SOLUTION TO MAGNETIC FIELD

Based on the medium type, the analytical model of the dual-core sensor can be divided into five solution domains. In each domain, the magnetic induction intensity (MII) consists of the tangential component $B_{i\varphi}$ and the normal component B_{ir}. The vector sum and its magnitude can be written as

$$\begin{cases} \vec{B}_i = B_{i\varphi}\vec{e}_\varphi + B_{ir}\vec{e}_r \\ \left|\vec{B}_i\right| = \sqrt{B_{i\varphi}^2 + B_{ir}^2}, \end{cases} \tag{1}$$

where $i = I, II, III, IV, V$. Detailed derivation and expression of B_i are provided in Appendix.

According to Eq. (A-5), these coefficients determine the magnetic field inside the sensor, which are associated with core properties, geometric parameters and conducting currents. For a specified industrial electrical asset of service, the property and geometric dimension of the cores and the cable positioning can be predetermined as appropriate. Hence, the magnetic field distribution in the whole domain is only dependent on the conducting currents in cables.

To clarify the filtering effect of the inner core, the following presents the analytical analysis in three scenarios respectively, where magnetic field distribution results from the load current only, the DM current only and the full conducting currents.

1) SCENARIO 1: NO DM CURRENT

When there is no DM current, namely the equal go and return currents in two cables, the currents can be defined as

$$I_1(t, \theta_1) = -I_2(t, \theta_2) = I_{1oad}\sin(\omega t), \tag{2}$$

where I_1 and I_2 are the amplitudes of two conducting currents in cables, and θ_1 and θ_2 are their phase angles that can be both assumed equal to 0°, and I_{load} and ω are the amplitude and angular frequency of the load current at power frequency.

According to the Appendix, $B_{i\varphi}$ and B_{ir} in two cores are

$$\begin{cases} B_{II\varphi}^{load} = -\dfrac{I_{1oad}\sin(\omega t)}{r}\displaystyle\sum_{n=1}^{\infty}\left[1-(-1)^{n+1}\right] \\ \qquad n(g_n r^n - h_n r^{-n})\cos n\varphi \\ B_{IIr}^{load} = -\dfrac{I_{1oad}\sin(\omega t)}{r}\displaystyle\sum_{n=1}^{\infty}\left[1-(-1)^{n+1}\right] \\ \qquad n(g_n r^n + h_n r^{-n})\sin n\varphi, \end{cases} \tag{3}$$

$$\begin{cases} B_{IV\varphi}^{load} = -\dfrac{I_{1oad}\sin(\omega t)}{r}\displaystyle\sum_{n=1}^{\infty}\left[1-(-1)^{n+1}\right] \\ \qquad n(k_n r^n - l_n r^{-n})\cos n\varphi \\ B_{IVr}^{load} = -\dfrac{I_{1oad}\sin(\omega t)}{r}\displaystyle\sum_{n=1}^{\infty}\left[1-(-1)^{n+1}\right] \\ \qquad n(k_n r^n + l_n r^{-n})\sin n\varphi. \end{cases} \tag{4}$$

The forms of Eq. (3) and Eq. (4) are highly consistent. They give a mathematical indication that in this scenario each core has a rotary dipole magnetic field distribution. Four coefficients g_n, h_n, k_n and l_n determine the difference between MIIs in two cores. In other words, the filtering effect relies on these four coefficients, which is the objective of the optimization design to confirm the geometric dimension of the sensor.

Using the specifications in Table. 1, the resultant MIIs in the inner core ($r = 40.5$ mm) and the outer core ($r = 63$ mm) are plotted in Fig. 3(a), where $I_{\text{load}} = 20$A. By comparing the results in two cores, it is discovered that the magnetic field in the outer core is weakened to be ten thousandth of that in the inner core.

2) SCENARIO 2: ONLY DM CURRENT

When there is only the DM current in a few milliamps in the inlet cable, the currents are modified as

$$\begin{cases} I_1(t, \theta_1) + I_2(t, \theta_2) = I_{diff}\sin(\omega t + \Delta\theta) \\ I_{1oad} = 0, \end{cases} \tag{5}$$

where I_{diff} represents the amplitude of DM current, and $\Delta\theta$ is the phase difference between the load current and the DM current.

In this scenario, $B_{i\varphi}$ and B_{ir} in two cores are

$$\begin{cases} B_{II\varphi}^{Diff} = \dfrac{I_{diff}\sin(\omega t + \Delta\theta)}{r} \\ \qquad \left[d\dfrac{u_r}{2\pi} - \displaystyle\sum_{n=1}^{\infty} n(g_n r^n - h_n r^{-n})\cos n\varphi\right] \\ B_{IIr}^{Diff} = -\dfrac{I_{diff}\sin(\omega t + \Delta\theta)}{r}\displaystyle\sum_{n=1}^{\infty} n(g_n r^n + h_n r^{-n})\sin n\varphi, \end{cases} \tag{6}$$

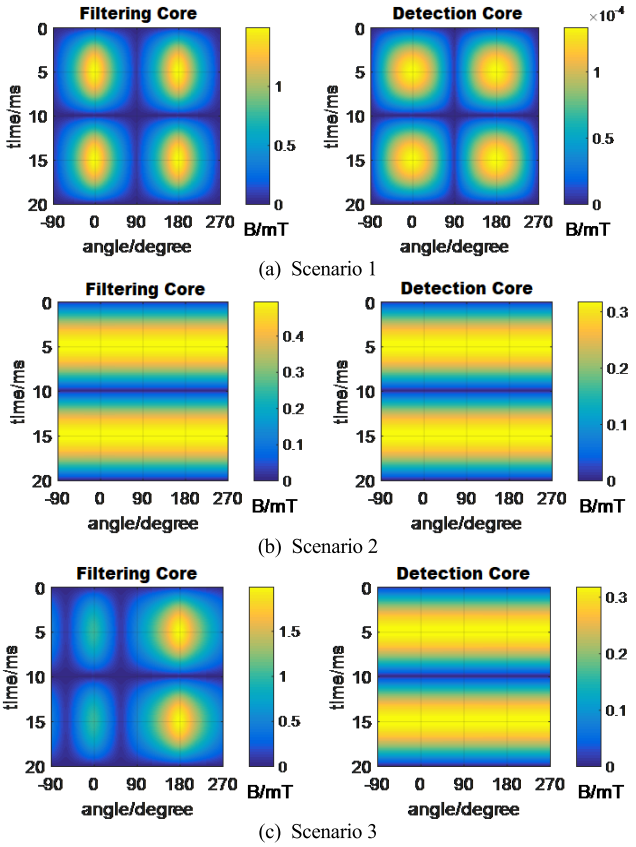

FIGURE 3. Magnetic field distributions in two cores in different scenarios.

$$\begin{cases} B_{\mathrm{IV}\varphi}^{Diff} = \dfrac{I_{diff}\sin(\omega t+\Delta\theta)}{r} \\ \qquad \left[\dfrac{u_r}{2\pi} - \displaystyle\sum_{n=1}^{\infty} n(k_n r^n - l_n r^{-n})\cos n\varphi\right] \\ B_{\mathrm{IV}r}^{Diff} = -\dfrac{I_{diff}\sin(\omega t+\Delta\theta)}{r}\displaystyle\sum_{n=1}^{\infty} n(k_n r^n + l_n r^{-n})\sin n\varphi. \end{cases} \tag{7}$$

As an example where $I_{\mathrm{diff}} = 1\mathrm{mA}$ and $\Delta\theta = 0°$, the resultant MIIs in two cores are plotted in Fig. 3(b). It can be observed that the magnetic field produced by the DM current distributes uniformly in both cores. Since the inlet cable conducting DM current is not placed in the center, it indicates that small current measurement using the regular single-core sensor is insensitive to cable positioning.

3) SCENARIO 3: DM CURRENT AND LOAD CURRENT

Based on the superposition principle, $B_{\mathrm{i}\varphi}$ and B_{ir} produced by the full conducting currents in two cables can be obtained using Eq. (3), Eq. (4), Eq. (6) and Eq. (7). They are

$$\begin{cases} B_{i\varphi} = B_{i\varphi}^{load} + B_{i\varphi}^{Diff} \\ B_{ir} = B_{ir}^{load} + B_{ir}^{Diff}, \end{cases} \tag{8}$$

where $i = II$ and IV.

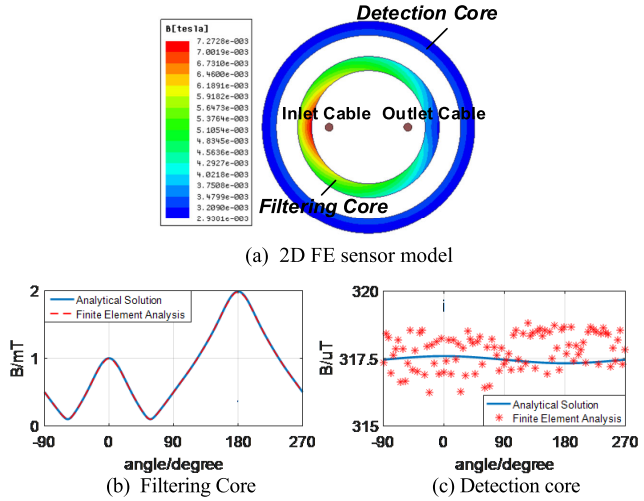

FIGURE 4. Comparison between analytical solution and 2D FEA in the filtering core and the detection core.

As shown in Fig. 3(c), the distribution is no longer symmetrical in the inner core. The magnetic field produced by large load current heavily masks that by the leakage current and leads to the asymmetry. It indicates that the DM measurement of a regular sensor can be affected due to its conventional single-core topology.

However, the inner core greatly confines the flux produced by the load current and achieves an effective filtering effect of the noises. As a result, DM current contributes to most of the flux in the outer core, which can distribute uniformly in a 360-degree circle. In combination with Fig. 3(b) and (c), the MIIs in the detection core are found basically the same under *Scenario 2* and *Scenario 3*.

In short, based on the specified example, the above analytical analysis clarifies the significance of the dual-core topology for the DM measurement. The filtering core realizes an effective reduction of strong load current noises. The SNR of measurement in the outer core can be significantly improved compared with that in the inner core.

C. FINITE ELEMENT ANALYSIS VALIDATION

In order to validate the proposed analytical model of the dual-core current sensor for DM current measurement, 2D FEA in Ansys/Maxwell is conducted using the same medium properties, geometric configuration and conducting currents as these in *Scenario 3*. The magnetic field distribution in the 2D FE sensor model is illustrated in Fig. 4 (a). Fig. 4 (b) and (c) present comparative results in the filtering and detection cores, respectively. In each group, the results from analytical solution and 2D FEA are in very close agreement.

Therefore, magnetic field distribution inside the sensor can be solved straight away based on the analytical model proposed in this section. The insulation requirement, the rated load current and the normal leakage current of the monitored asset are typically specific. On this basis, the model can

greatly benefit the sensor design, as a trade-off between the geometric dimension and the SNR of measurement.

III. ANALYTICAL ANALYSIS OF OPERATING EFFECTS

In the previous section, analytical solution to magnetic field distribution of the dual-core sensor is presented on ideal assumptions. But for the field implementation, the accuracy and sensitivity of DM measurement are subject to several operating factors. *Firstly*, power system operates with changeable power factor and load condition. *Secondly*, some defects probably exist in the process of the manufacture and installation. Asymmetry in cable positioning may alter magnetic field distribution in cores. *Thirdly*, the filtering effect is dependent on the axial length of the inner core.

A. EFFECTS OF PHASE DIFFERENCES BETWEEN THE CURRENTS

Fig. 5 gives the phasor diagram of variables at power frequency. There is a phase difference of dielectric loss angle (δ) between the operating voltage (U) and the leakage current (I_{leak}). Insulation ageing leads to a very slow ascent of δ ranging in a few degrees. By contrast, the phase difference between U and the load current (I_{load}), defined as power factor angle (γ), may change significantly due to fluctuating operation of power system. As a result, the total phase difference ($\Delta\theta$) between I_{load} and I_{leak} has a real-time variation in an uncertain range.

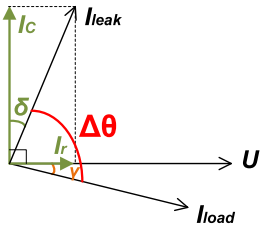

FIGURE 5. Phasor diagram of the load current and the leakage current.

In general, the insulation system of the asset has a δ close to 0°. Assuming the power factor of the system is nearly 0.8, $\Delta\theta$ can be set between 90° to 130° for the analysis. Fig. 6 presents analytical results by changing $\Delta\theta$ in Eq. (5). It is discovered that magnetic field distribution in the inner core is position-dependent around the circle. Across the areas centered at $\varphi = 0°$ and $\varphi = 180°$, the MII is heavily affected by $\Delta\theta$. By contrast, it remains almost unchanged in 360-degree circle of the detection core, under any circumstance of $\Delta\theta$ ranging from 90° to 130°.

B. EFFECTS OF LOAD CURRENT AMPLITUDE

Fluctuation in system operation can cause changes to the amplitude of the load current. A computational evaluation is performed by changing I_{load} from 0 to 100A while keeping I_{diff} and $\Delta\theta$ equal to 1mA and 110°, respectively. The results are plotted in Fig. 7. I_{load} and the MII have an obvious positive

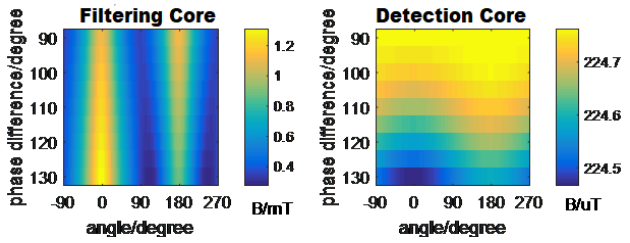

FIGURE 6. Magnetic field distributions in two cores under the circumstances of different $\Delta\theta$.

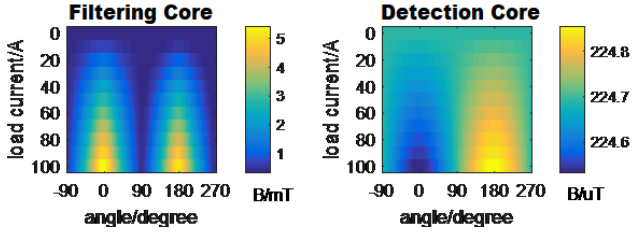

FIGURE 7. Magnetic field distributions in two cores under the circumstances of different I_{load}.

correlation at the positions of $\varphi = 0°$ and $\varphi = 180°$ of the inner core. However, the MII is almost constant at any position in the outer core.

The analysis in Section III-A and B can demonstrate the effect of system operation on the performance of the regular single-core sensor. The load-dependent feature is the crucial reason for its low-sensitivity measurement. By contrast, for the proposed sensor with dual-core topology, the inner core plays a significant role in filtering strong load current noises. The variation of either $\Delta\theta$ or I_{load} has little impact on the MII in the outer core. Hence, DM current measurement of the proposed sensor is proven robust to system operation.

C. EFFECTS OF ASYMMETRY IN CABLE POSITIONING

There may be a slight asymmetry in cable positioning during the manufactory and installation process. As shown in Fig. 8(a), ten groups of cable positioning are simulated, where the inlet cable is configured with different degrees of slight asymmetry relative to the outlet cable. In these cases, I_{load} is 20A. I_{diff} and $\Delta\theta$ are kept at 1mA and 110°, respectively.

Fig. 8(b) shows the computed results of three points at each core, whose φ are equal to 0°, 90° and 180°. It is discovered that a slight asymmetry can cause a significant change of the MII in the inner core. Nevertheless, due to the effective filtering effect, the MII of each specified point in the detection core remains constant under all cases of different degrees of positioning asymmetry. Hence, the performance of the dual-core sensor is validated with little influence of asymmetry in cable positioning.

D. EFFECTS OF AXIAL LENGTH OF FILTERING CORE

The analytical model and 2D FE model are built based on the assumption that the lengths of cores and cables are

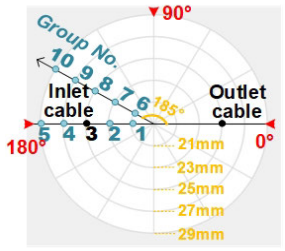

(a) Geometric illustration of asymmetrical cable positioning

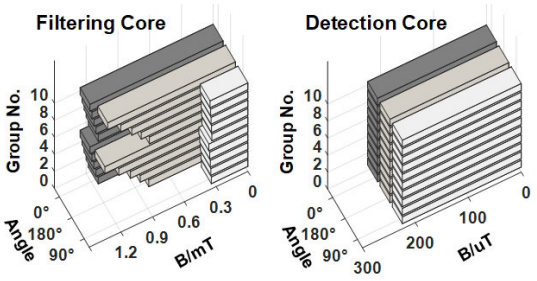

(b) Analytical results

FIGURE 8. Magnetic field distributions in two cores under the circumstances of different cable positions.

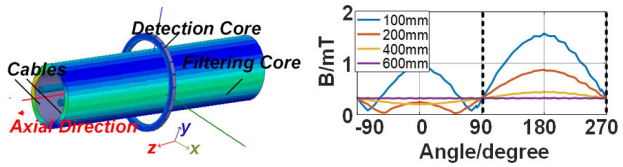

(a) 3D FE model (b) 3D FE results of the outer core

FIGURE 9. Magnetic field distributions when L_z is different.

TABLE 2. Simulation conditions in 3D FE model.

Unit	Axial Length (L_z)
Cables	600 mm
Detection Core	10 mm
Filtering Core	100, 200, 400, 600 mm

infinite. In practice, the sensor has a limited axial length, which may change the magnetic field distribution in the cores. To illustrate such an effect, a 3D FE model is built as shown in Fig. 9 (a). Four groups of simulation are conducted under different axial lengths of the filtering core (L_z) as listed in Table 2. The radial dimension and conducting currents are set the same as those in the 2D FE model.

According to Fig. 9 (b), L_z not only influences the MII but also changes the degree of non-uniformity of magnetic field distribution in the detection core. The shorter L_z is, the more non-uniformly magnetic field distributes around the 360-degree circle. It indicates the reason why the performance of the earlier-designed sensor in [17] is affected by the non-uniformity of the full-circle wrapped coil.

Therefore, to improve the measurement accuracy of the proposed dual-core sensor, it is vital to select an appropriate axial length of the inner core, along with an optimal approach for magnetic field detection in the outer core.

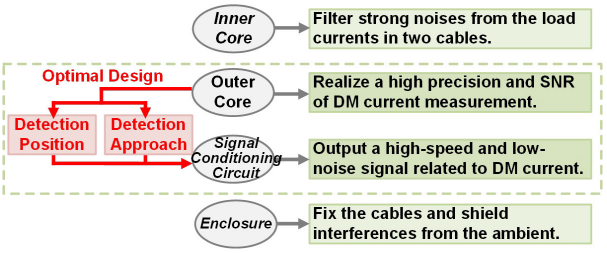

FIGURE 10. Function of four parts of the proposed sensor.

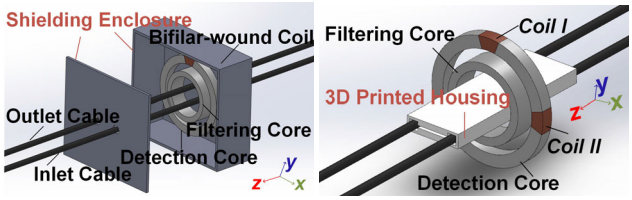

(a) Production version (b) Experimental version

FIGURE 11. Design graphics of the proposed current sensor.

IV. DESIGN PROCEDURE OF THE PROPOSED CURRENT SENSOR

The proposed sensor consists of four parts, *i.e.*, the filtering core, the detection core, the signal conditioning circuit, and the shielding enclosure. The significant function of each part is clarified in Fig. 10.

Previous sections have clarified the significant role analytically that the inner filtering core plays. The enclosure in the production version, as shown in Fig. 11(a), accomplishes two main functions. In the experimental version in Fig. 11(b), the enclosure is not included. Instead, a 3D printed housing is used for cable positioning. This section aims at achieving a comprehensive design procedure, by carefully investigating the optimal position and approach to detecting the magnetic field caused by DM current.

A. OPTIMAL DETECTION POSITION

Section III-D indicates that magnetic field distribution in the outer core is affected by the axial dimension of the filtering core. However, it is worth noting that, the MII remains unchanged with any L_z in the axisymmetric line of the inlet and outlet cables in XY-plane. In other words, at the position of the outer core where φ is equal to 90° or 270°, the MII caused by DM current can be detected with the least noises in the presence of large load current. Hence, either position is optimal for the DM measurement.

B. OPTIMAL DETECTION APPROACH

Based on the optimal detection position, the next is to select an optimal approach for magnetic field detection. By careful comparison among several popularly-applied approaches, the sensor adopts the detection approach based on the zero-flux principle, as described in Fig. 12. A bifilar-wound coil, which consists of the detection coil and the compensation coil, achieves a dynamic and prompt field detection inside the core. The key factors considered are discussed as follows.

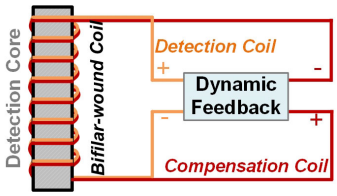

FIGURE 12. Magnetic field detection based on the zero-flux principle.

Firstly, it enables a *high-speed* response to magnetic field variation. Once the measured DM current changes, the compensation coil can immediately give a reversed induced electromotive force of the detection coil via the dynamic feedback block. The feedback speed is typically less than a microsecond. The flux in the detection core can always maintain a near-zero state as a result.

Secondly, it enables a *high-sensitivity* measurement under the mask of strong noises. After filtering noises by the inner core, the weak flux produced by DM current is well confined to the detection core with little flux leakage. Any slight change in the DM current can be reflected sensitively. By contrast, if an embedded magnetic sensor is used, the sensitivity could be significantly reduced due to the flux leakage and noises in the air gap of the core.

Thirdly, it helps reduce the effect of non-idealities of the secondary winding. The detection based on the current transforming principle requires a mass of turns (up to several thousand). Measurement errors may result from the non-uniformity and the resistance of the winding. By contrast, the zero-flux-based detection using the bifilar-wound coil can avoid this problem. Moreover, the turn number is relatively small that can be optimized as a trade-off between the detection sensitivity and the driving voltage of the signal conditioning circuit.

C. SIGNAL CONDITIONING CIRCUIT

Fig. 13 provides the block diagram of the designed simple integrated signal conditioning circuit, which serves to output a high-speed and low-noise signal of the milliampere-level DM current. The induced current in detection coil transfers from the primary current, whose value is reduced by the turn-number (N_{turns}) times. After the DC-blocking filter, the current is amplified A_{f} times via a two-stage amplifier using Opa2227. Then, the output signal is given by the computing unit.

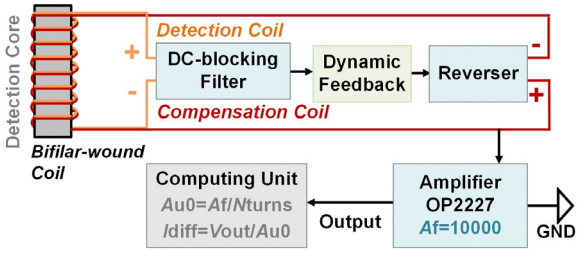

FIGURE 13. Block diagram of the signal conditioning circuit.

The output performance of the circuit depends on the type of used amplifier. Opa2227 is an operational amplifier with characteristics of low noise ($3\text{nV}/\sqrt{\text{Hz}}$), wide band width (8MHz) and low offset voltage (75uV). The delay of electronic components and the computing speed are generally less than a microsecond. Such a fast duration is sufficient to ensure the DM current measurement at power frequency.

D. GEOMETRIC CONFIGURATION

Based on the above comprehensive considerations, the dual-core current sensor can be elaborately designed for a specified monitoring background. A sensor prototype is built for laboratory validation, with a view to the industrial application of the medium electrical machine. The insulation distance between two cables is 50 mm. The load current is up to 100A and the DM current ranges from 0 to 7mA. The tested sensor has the radial dimensions as listed in Table. 1. The material of two cores is permalloy whose initial permeability is around $4\pi \times 10^{-3}$H/m. The axial length of the inner and outer cores is 10mm and 18mm, respectively. Two cables with 25mm^2 cross-sectional area are placed into the 3D printed housing to ensure the positioning as symmetrical as possible.

As illustrated in Fig. 11(b), the bifilar-wound coil is wrapped around a local region of the outer core centered at $\varphi = 90°$, which is named as *Coil I*. Another group of the bifilar-wound coil (*Coil II*) is wrapped around the region centered at $\varphi = 0°$, in order to figure out magnetic field difference associated with the detection position. In addition, the value of N_{turns} is crucial to the performance. If it is too small, the driving voltage would be insufficient for the amplifier. Yet the width of the coil should be as narrow as possible to reduce load current noises to the lowest possible level. After a reasonable compromise, N_{turns} is set to 500 and the coil width is about 20mm in the prototype.

V. EXPERIMENTAL STUDY

A. EXPERIMENTAL SETUP

According to the schematic in Fig. 14(a), experiments are carried out to validate the performance of the prototype for DM current measurement. The setup in the laboratory is shown in Fig. 14(b). The large current generator *HPU PTC-8300D* can generate a controlled load current from 0 to 100A. The circuit consisting of the signal generator *RIGOL DG4062* and a 1kΩ resistance can generate small DM current in the range of 0-7mA.

In this way, $\Delta\theta$ of each test is not constant due to the random trigger angle of the signal generator. This series of experimental results can show whether the results of two coils are affected by $\Delta\theta$ due to the system fluctuation.

In addition, another series of experiments are conducted with a fixed $\Delta\theta$, by referencing the schematic as shown in Fig. 14(c). The DM current is transformed directly from the load current using the current transformer (CT) with the ratio 100A:1A. Assuming the CT has a constant transferring

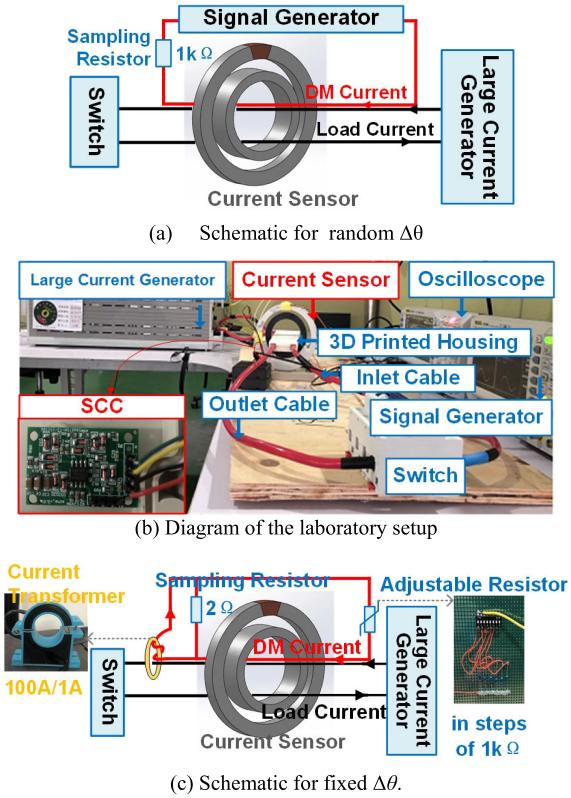

(a) Schematic for random $\Delta\theta$

(b) Diagram of the laboratory setup

(c) Schematic for fixed $\Delta\theta$.

FIGURE 14. Experimental setups and schematic diagrams.

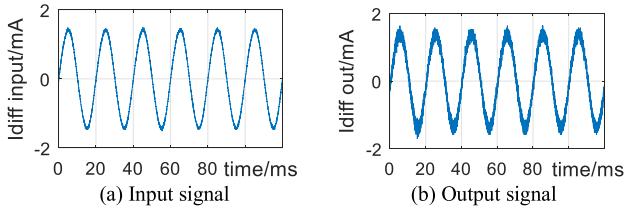

(a) Input signal (b) Output signal

FIGURE 15. Experimental results of *Coil I* when I_{load} = 50A and I_{diff} = 1.414mA.

angle error, $\Delta\theta$ remains the same in each test. I_{diff} is adjusted by changing the resistor on the secondary side.

B. EXPERIMENTS CONDUCTED UNDER RANDOM $\Delta\theta$

A series of experiments are conducted according to Fig. 14(a). In this scenario, $\Delta\theta$ is randomly chosen to simulate the fluctuation in system operation. Fig. 15(a) and (b) show a group of the input and output signals of the sensor when I_{load} = 50A and I_{diff} = 1.414mA. The input signal uses the measured voltage on the sampling resistor as a reference.

Fig. 16 (a) presents a set of curves describing a linear relation between the output and input signals. The linearity is unaltered under different load currents. As shown in Fig. 16 (b), the errors of the output signals are calculated with respect to the referenced inputs. They are kept below 0.1mA. In Fig. 16(c), when I_{diff} is larger than 0.5mA, the sensor displays the output with a small percentage error.

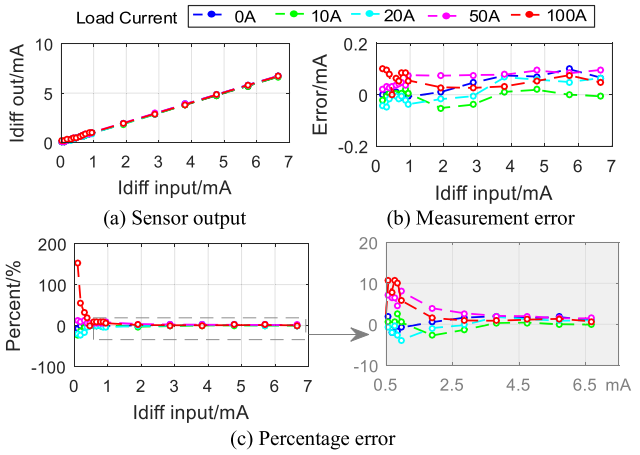

(a) Sensor output (b) Measurement error

(c) Percentage error

FIGURE 16. Experimental results of *Coil I* under different input signals.

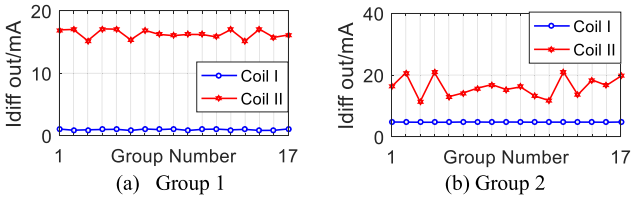

(a) Group 1 (b) Group 2

FIGURE 17. Experimental results at various observing times in Group 1 (I_{load} = 50A and I_{diff} = 1.414mA), and Group 2 (I_{load} = 50A and I_{diff} = 7.07mA).

When I_{diff} is smaller than 0.5mA, the percentage error tends to be larger, which can be interpreted in two parts. *For one thing*, the shielding enclosure is not included in the prototype. The output is liable to be influenced by the ambient interferences. *For another*, the length of the cables is about one meter in the experiment. They are not strictly placed in parallel using the 3D printed housing, as shown in Fig. 14(b). In the production version, the measurement precision can be further improved, by adding the shielding enclosure and making delicate positioning of the cables.

The following two groups of experiments are carried out to validate the optimal detection region over the outer core. In Fig. 17, the outputs of *Coil I* and *Coil II* are recorded 17 times. At each observation, the output of *Coil I* maintains a stable value associated with the input whereas the output of *Coil II* fluctuates randomly. Hence, the accuracy of DM current measurement is relevant to the coil position. *Coil I* can perform the highest SNR of measurement under different system operations.

C. EXPERIMENTS CONDUCTED UNDER FIXED $\Delta\theta$

These series of experiments are conducted based on Fig. 14(c). In this scenario, since the input DM current is determined by the load current, $\Delta\theta$ remains at zero. The ratio of I_{diff} to I_{load} is from 0.02‰ to 0.07‰ in steps of 0.01‰, according to the step of the adjustable resistor.

In Fig. 18 (a), the curves describing the relation between the input DM current and the output of *Coil I* are linear and consistent. Meanwhile, each curve of *Coil II* has a certain

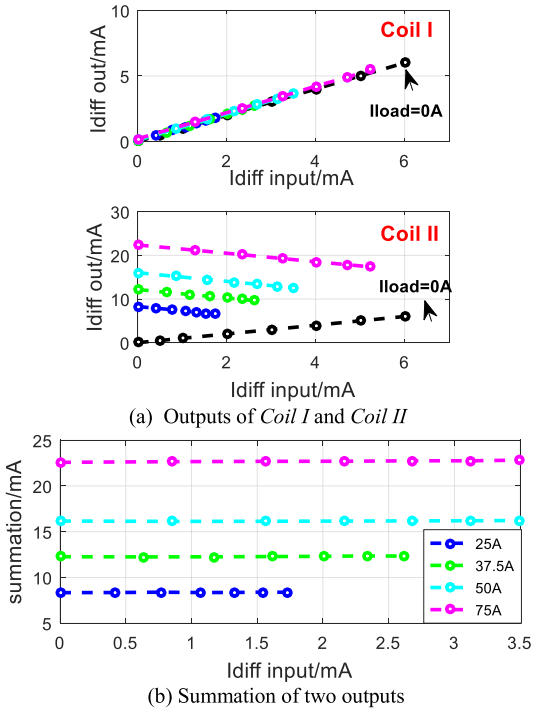

(a) Outputs of *Coil I* and *Coil II*

(b) Summation of two outputs

FIGURE 18. Experimental results under fixed $\Delta\theta$.

bias varying with I_{load}. By adding the outputs of *Coil I* and *Coil II*, the summation is shown in Fig. 18 (b). These curves are parallel, whose magnitudes are independent of the input I_{diff} but are proportional to the input I_{load}.

The result in Fig. 18(b) can be explained using analytical expressions in Section II. In combination with Eq. (4), Eq. (7) and Eq. (8), the summation of two outputs can be expressed as

$$\begin{aligned} B_{\text{IV}}^{summation} &\approx -\frac{I_{1oad}\sin(\omega t)}{r}\sum_{n=1}^{\infty}\left[1-(-1)^{n+1}\right]n(k_n r^n - l_n r^{-n}) \\ &= B_{\text{IV}\varphi}^{load}\Big|_{\varphi=0^\circ}, \end{aligned} \tag{9}$$

which relies on two assumptions, *i.e.*, ignoring the rather small normal components and $I_{\text{load}} \gg I_{\text{diff}}$.

Eq. (9) evidences that, in addition to geometric parameters, the summation of two outputs is only decided by I_{load} but irrelevant to I_{diff}. Therefore, by taking advantage of the results of two coils, the load condition of the monitored asset is available and worthy of further study.

In short, the above experimental results demonstrate two points. *For one thing*, system fluctuation has strong impact on magnetic field distribution. *Coil I* is preferably selected to prevent being affected by changeable $\Delta\theta$ and I_{load}. *For another*, the proposed dual-core current sensor is verified for the milliampere-level DM current measurement under strong load current noises.

TABLE 3. Instructions of two industrial current sensors for comparison.

Description	*Sensor 1*	*Sensor 2*
Manufacturer	ETCR/China	NBET Co./China
Product Model	Clamp Leaker 6300	BNWXL-110W
Measurement range	1 uA --60A	0 --1A
Accuracy	±1.5 %	0.1 %
Dimension	25*30 mm	117 mm (inner diameter)
Core topology	Single core with an air gap	Closed single core
Detection Principle	Magnetic sensor	Zero-flux principle (full-circled secondary coils)

D. COMPARATIVE EXPERIMENTS WITH INDUSTRIAL SENSORS

To clarify the superiority of the proposed sensor, comparative experiments are further conducted with two industrial products, whose instructions are given in Table 3. They are conventionally for leakage current measurement in practice but have different core topology and detection principle from these of the proposed sensor.

Sensor 1 adopts a magnetic sensor embedded in the core for magnetic field detection. Fig. 19 illustrates the test display and experimental results. The curves show a linear feature associated with the DM current. However, the error gradually increases as a result of increasing load current. In addition, the small dimension limits the application of per-phase monitoring, where two cables should be positioned in the consideration of appropriate insulation distance.

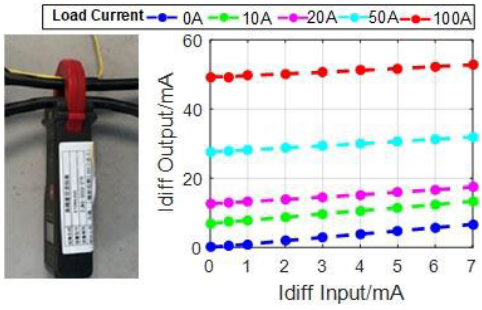

FIGURE 19. Test display and experimental results of *Sensor 1*.

Sensor 2 has the same radial dimension with that of the outer core of the sensor prototype. It also adopts the zero-flux principle, but the bifilar-wound coil is fully circled around the core. The test display and experimental results are presented in Fig. 20. Strong load current noises have an obvious impact on the performance. Some points of the curves close to zero show a nonlinear characteristic. This is due to the measurement by the full-circled secondary coil can be affected by load conditions.

It is notable that both industrial sensors only show satisfactory performances when there is only the DM current in two cables, as plotted in dark-blue lines in Fig. 19 and Fig. 20. However, when the cables conduct large load current, they fail to measure the DM current with high accuracy and

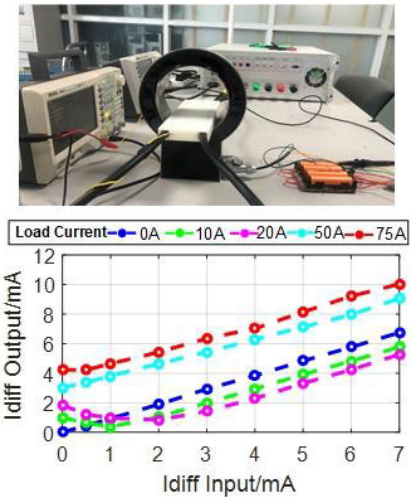

FIGURE 20. Test display and experimental results of *Sensor 2*.

sensitivity. It greatly owes to their single-core topology that cannot reduce load current noises effectively.

Hence, in combination with comparative experiments, the proposed dual-core sensor has been validated for the milliampere-level DM current measurement.

VI. CONCLUSION

Advanced measurement unit is under expansion in modern power system to allow a broader coverage of insulation monitoring of industrial electrical assets. This article has proposed an advanced DM sensor with the dual-core topology, which enables a high accuracy and sensitivity of leakage current measurement under strong load current noises.

In this article, an analytical model of the magnetic field distribution has been provided to clarify the filtering effect of the inner core. For the illustrated example, the load current noises are reduced by 10^{-4} times and the SNR of DM current measurement is greatly increased. Moreover, analytical results have validated the proposed sensor with little influence of system fluctuation and asymmetrical cable positioning. Besides, a comprehensive design procedure has been presented, by selecting the optimal detection position and approach and providing the high-speed and low-noise signal conditioning circuit. Experimental results have validated that the prototype has the measurement error within 0.1mA when the load current is up to 100A and the DM current varies from 0-7mA. The superior performance has been further stated in comparison with two industrial sensors.

According to the proposed analytical model and design procedure, the contribution of this article lies in improving the performance of the sensor in measuring the milliampere-level leakage current. Online per-phase insulation monitoring for industrial electrical assets can be implemented in a reliable and accurate manner.

APPENDIX

Here describes the derivation process of magnetic field distribution in the whole solution domain in Fig. 2, where a single cable extends through the dual-core sensor with the conducting current I.

According to the electromagnetic theory, magnetic scalar potentials in five solution domains can be expressed as

$$\begin{cases} A_{\mathrm{I}z} = -u_0 I \\ A_{\mathrm{II}z} = A_{\mathrm{III}z} = A_{\mathrm{IV}z} = A_{\mathrm{V}z} = 0. \end{cases} \tag{A-1}$$

Their directions are the same with the direction of the conducting current, which are all perpendicular to the plane of polar coordinates. Based on the separation variable method and the uniqueness theorem, Eq. (A-1) can be solved by considering the definite solution condition. Magnetic scalar potentials at any location coordinate (r, φ) are obtained as

$$\begin{cases} A_{\mathrm{I}z} = -\frac{u_0 I}{2\pi}\ln r + \frac{u_0 I}{2\pi}\sum_{n=1}^{\infty}(\frac{b}{r})^n \frac{1}{n}\cos n(\varphi-\varphi_0) \\ \qquad\qquad + \cdots + \sum_{n=1}^{\infty} e_n r^n \cos n(\varphi-\varphi_0) \\ A_{\mathrm{II}z} = \sum_{n=1}^{\infty}(g_n r^n + h_n r^{-n})\cos n(\varphi-\varphi_0) + h_0 \ln r \\ A_{\mathrm{III}z} = \sum_{n=1}^{\infty}(i_n r^n + j_n r^{-n})\cos n(\varphi-\varphi_0) + j_0 \ln r \\ A_{\mathrm{IV}z} = \sum_{n=1}^{\infty}(k_n r^n + l_n r^{-n})\cos n(\varphi-\varphi_0) + l_0 \ln r \\ A_{\mathrm{V}z} = \sum_{n=1}^{\infty} m_n r^{-n}\cos n(\varphi-\varphi_0) + m_0 \ln r, \end{cases} \tag{A-2}$$

where e_{n}, g_{n}, h_{n}, i_{n}, j_{n}, k_{n}, l_{n}, m_{n}, h_0, j_0, l_0, m_0 are the evaluated coefficients, and (b, φ_0) is the location coordinate of the cable.

Then, the MII in each solution domain can be obtained using the relationship

$$\begin{cases} B_{i\varphi} = \dfrac{1}{r}\dfrac{\partial A_{iz}}{\partial \varphi} \\ B_{ir} = -\dfrac{\partial A_{iz}}{\partial r} \end{cases} \qquad i = I, II, III, IV, V. \tag{A-3}$$

According to the boundary conditions

$$\begin{cases} B_{ir} = B_{jr} \\ B_{i\varphi}/\mu_i = B_{j\varphi}/\mu_j \end{cases} \qquad i, j = I, II, III, IV, V (i \neq j). \tag{A-4}$$

The relationships among these coefficients are obtained as

$$h_0 = -\frac{u_r I}{2\pi},\quad j_0 = -\frac{u_0 I}{2\pi},\quad l_0 = -\frac{u_r I}{2\pi},\quad m_0 = -\frac{u_0 I}{2\pi},$$
$$k_n = \frac{1-u_r/u_0}{2} q^{-2n} m_n,\ l_n = \frac{1+u_r/u_0}{2} m_n,$$
$$i_n = \frac{1+u_0/u_r}{2} k_n + \frac{1-u_0/u_r}{2} p^{-2n} l_n,$$
$$j_n = \frac{1-u_0/u_r}{2} p^{2n} k_n + \frac{1+u_0/u_r}{2} l_n,$$

$$g_n = \frac{1+u_r/u_0}{2} i_n + \frac{1-u_r/u_0}{2} c^{-2n}$$
$$j_n, h_n = \frac{1-u_r/u_0}{2} c^{2n} i_n + \frac{1+u_r/u_0}{2} j_n. \quad \text{(A-5)}$$

Substituting Eq. (A-5) into $B_{\mathrm{I}\varphi} = B_{\mathrm{II}\varphi}$, these coefficients can be solved, which are expressed by core properties, geometric parameters and conducting currents. Then, substituting them into the expressions of MII in Eq. (A-3), magnetic field distribution in the whole solution domain caused by the single conducting current is obtained analytically. Under the circumstance of two cables extending through the sensor, analytical expressions can be further obtained based on the superposition principle.

REFERENCES

[1] K. Moslehi and R. Kumar, "A reliability perspective of the smart grid," *IEEE Trans. Smart Grid*, vol. 1, no. 1, pp. 57–64, Jun. 2010.

[2] A. Bellini, F. Filippetti, G. Franceschini, C. Tassoni, R. Passaglia, M. Saottini, G. Tontini, M. Giovannini, and A. Rossi, "On-field experience with online diagnosis of large induction motors cage failures using MCSA," *IEEE Trans. Ind. Appl.*, vol. 38, no. 4, pp. 1045–1053, Jul. 2002.

[3] Motor Reliability Working Group, Power Systems Reliability Subcommittee, Power Systems Engineering Committee; Industrial & Commercial Power Systems Department, and IEEE Industry Applications Society, "Report of large motor reliability survey of industrial and commercial installations: Part 3," *IEEE Trans. Ind. Appl.*, vol. IA-23, no. 1, pp. 153–158, Jan. 1987.

[4] F. Dixon, D. Steward, and J. Hoffmeister, "When to replace aging transformers: Guidelines to replace older transformers before failure," *IEEE Ind. Appl. Mag.*, vol. 18, no. 5, pp. 46–56, Sep. 2012.

[5] S. Tenbohlen, J. Jagers, and F. Vahidi, "Standardized survey of transformer reliability: On behalf of CIGRE WG A2.37," in *Proc. Int. Symp. Electr. Insulating Mater. (ISEIM)*, Sep. 2017, pp. 593–596.

[6] P. Shede and S. Mane, "Leakage current sensing techniques," in *Proc. 3rd Int. Conf. Sens., Signal Process. Secur. (ICSSS)*, May 2017, pp. 181–185.

[7] P. Zhang, P. Neti, and K. Younsi, "Online monitoring of capacitance and dissipation factor of motor stator winding insulation during accelerated life testing," in *Proc. IEEE Energy Convers. Congr. Expo. (ECCE)*, Sep. 2018, pp. 3267–3271.

[8] G. Faria, M. Pereira, G. Lopes, J. Villibor, P. Tavares, and I. Faria, "Evaluation of capacitance and dielectric dissipation factor of distribution transformers–experimental results," in *Proc. IEEE Electr. Insul. Conf. (EIC)*, Jun. 2018, pp. 336–339.

[9] I. Tsyokhla, A. Griffo, and J. Wang, "On-line monitoring of winding insulation health using high frequency common mode voltage from PWM," in *Proc. IEEE Int. Electr. Mach. Drives Conf. (IEMDC)*, May 2015, pp. 1433–1439.

[10] P. Neti and S. Grubic, "Online broadband insulation spectroscopy of induction machines using signal injection," *IEEE Trans. Ind. Appl.*, vol. 53, no. 2, pp. 1054–1062, Mar. 2017.

[11] I. Tsyokhla, A. Griffo, and J. Wang, "Detection of humidity ingress using online common-mode insulation impedance-monitoring system," *J. Eng.*, vol. 2019, no. 17, pp. 4411–4414, Jun. 2019.

[12] I. Tsyokhla, A. Griffo, and J. Wang, "Online condition monitoring for diagnosis and prognosis of insulation degradation of inverter-fed machines," *IEEE Trans. Ind. Electron.*, vol. 66, no. 10, pp. 8126–8135, Oct. 2019.

[13] G. Stone, "Condition monitoring and diagnostics of motor and stator windings—A review," *IEEE Trans. Dielectr. Electr. Insul.*, vol. 20, no. 6, pp. 2073–2080, Dec. 2013.

[14] P. Zhang, K. Younsi, and P. Neti, "A novel online stator ground-wall insulation monitoring scheme for inverter-fed AC motors," *IEEE Trans. Ind. Appl.*, vol. 51, no. 3, pp. 2201–2207, May 2015.

[15] S. Bin Lee, J. Yang, K. Younsi, and R. Bharadwaj, "An on-line groundwall and phase to phase insulation quality assessment technique for AC machine stator windings," in *Proc. Fourtieth IAS Annu. Meeting. Conf. Rec. Ind. Appl. Conf.*, Oct. 2005, pp. 10–19.

[16] W. R. Jensen, E. G. Strangas, and S. N. Foster, "A method for online stator insulation prognosis for inverter-driven machines," *IEEE Trans. Ind. Appl.*, vol. 54, no. 6, pp. 5897–5906, Nov. 2018.

[17] P. Neti, K. Younsi, and M. R. Shah, "A novel high sensitivity differential current transformer for online health monitoring of industrial motor ground-wall insulation," in *Proc. IEEE Energy Convers. Congr. Expo.*, Sep. 2013, pp. 2493–2499.

[18] W. Chen, C. Yao, P. Chen, C. Sun, L. Du, and R. Liao, "A new broadband microcurrent transducer for insulator leakage current monitoring system," *IEEE Trans. Power Del.*, vol. 23, no. 1, pp. 355–360, Jan. 2008.

[19] S. C. Oliveira, E. Fontana, and F. J. do Monte de Melo Cavalcanti, "Real-time monitoring of the leakage current of 230-kV glass-type insulators during washing," *IEEE Trans. Power Del.*, vol. 24, no. 4, pp. 2257–2260, Oct. 2009.

[20] M. M. Werneck, D. M. dos Santos, C. C. De Carvalho, F. V. B. de Nazare, and R. C. da Silva Barros Allil, "Detection and monitoring of leakage currents in power transmission insulators," *IEEE Sensors J.*, vol. 15, no. 3, pp. 1338–1346, Mar. 2015.

GEYE LU (Student Member, IEEE) received the B.S. and M.S. degrees in electrical engineering from North China Electric Power University, in 2014 and 2017, respectively. She is currently pursuing the Ph.D. degree with Tsinghua University. Her research for the master's degree is relay protection of the transformer in UHV power systems. Her current research interests are the condition monitoring techniques for transformer reliability improvement applied in power systems, converter systems, and renewable energy systems.

YANG WU (Graduate Student Member, IEEE) received the B.S. degree in electrical engineering from Tsinghua University, Beijing, China, in 2017, where she is currently pursuing the Ph.D. degree in electrical engineering. Her research interests include noninvasive measurement and condition monitoring of power systems and electrical assets.

PINJIA ZHANG (Senior Member, IEEE) received the B.Eng. degree in electrical engineering from Tsinghua University, Beijing, China, in 2006 and the master's and Ph.D. degrees in electrical engineering from the Georgia Institute of Technology, Atlanta, GA, USA, in 2009 and 2010, respectively. From 2010 to 2015, he was with the Electrical Machines Laboratory, GE Global Research Center, Niskayuna, NY, USA. Since 2015, he has been with the Department of Electrical Engineering, Tsinghua University, as an Associate Professor. He has published more than 80 papers in refereed journals and international conference proceedings, has more than 40 patent fillings in the U.S. and worldwide. His research interests include condition monitoring, diagnostics, and prognostics techniques for electrical assets. He was a recipient of IAS Andrew W. Smith Outstanding Young Member Achievement Award in 2018. He also received three best paper awards from the IEEE IAS and IES society.